

# We are IntechOpen, the world's leading publisher of Open Access books Built by scientists, for scientists

6,900

Open access books available

186,000

International authors and editors

200M

Downloads

Our authors are among the

154

Countries delivered to

TOP 1%

most cited scientists

12.2%

Contributors from top 500 universities



WEB OF SCIENCE™

Selection of our books indexed in the Book Citation Index  
in Web of Science™ Core Collection (BKCI)

Interested in publishing with us?  
Contact [book.department@intechopen.com](mailto:book.department@intechopen.com)

Numbers displayed above are based on latest data collected.  
For more information visit [www.intechopen.com](http://www.intechopen.com)



# SVR Controller for a Biped Robot with a Human-like Gait Subjected to External Sagittal Forces

João P. Ferreira<sup>2,1</sup>, Manuel Crisóstomo<sup>1</sup>,  
A. Paulo Coimbra<sup>1</sup> and Bernardete Ribeiro<sup>3</sup>

<sup>1</sup>*Institute of Systems and Robotics, Dept. of Electrical and Computer Engineering,  
Univ. of Coimbra,*

<sup>2</sup>*Dept. of Electrical Engineering, Superior Institute of Engineering of Coimbra, Coimbra,*

<sup>3</sup>*CISUC, Dept. of Informatics Engineering, Univ. of Coimbra, Coimbra,  
Portugal*

## 1. Introduction

This paper describes the control of a biped robot that uses an SVR (Support Vector Regression) for its balance. The control system was tested subjected to external sagittal pulling and pushing forces. Biped robots have leg link structures similar to the human's anatomy. To be able to maintain its stability under dynamic situations such robotic systems require good mechanical designs and force sensors to acquire the zero moment point (ZMP). Research in biped robotics has recently had a great surge due to the challenges of the subject and the media impact of famous biped robots like Honda's.

(Vukobratovic, 1990) developed a mathematical model of a biped robot and its method of control. Some research works (Zarrugh & Radcliffe, 1979), (Nakamura et al., 2004), (Jang et al., 2002) have reported the gait of biped robots based on human kinematics data, and a very good study of human body kinematics was done by Winter (Winter, 1990). Because a biped robot is easily knocked down, its stability must be taken into account in its gait design. Zheng (Zheng & Shen, 1990) proposed a method of gait synthesis taking into account the static stability. Chevallereau (Chevallereau et al., 1998) discussed dynamic stability through the analysis of the reaction force between the base of the foot and the ground. Unfortunately the defined trajectory does not assure the satisfaction of the stability restriction.

To assure the dynamic stability of a biped robot, Shin (Shin et al., 1990) and Hirai (Hirai et al., 1998) proposed standard methods for gait synthesis based on the zero moment point (ZMP). Basically this method consists of designing a desired ZMP trajectory, duly correcting the movement of the torso to maintain the ZMP trajectory as designed. However, because the change of the ZMP to accommodate the movement of the torso is limited, not all desired ZMP trajectories are possible (Park & Kim, 1998). The ZMP position can be obtained computationally using a model of the robot. However there might be a significant difference between the real and the calculated ZMP due to the difference between the real robot's physical parameters and its approximated mathematical model. To avoid this error, four force sensors are usually used on each foot to obtain an estimate for the real ZMP.

In the simplified 2-link control model the biped robot is divided into two masses, the torso and the legs, and can be used online. In the method described in this work the robot is divided into 8 links, which increases the accuracy, but also increases the computation time making it difficult to be used online. To overcome this limitation, some researchers propose computational intelligence techniques such as neuro-fuzzy nets and fuzzy systems for the control of biped robots (Choi et al., 2006), (Behnke, 2006), (Ferreira et al., 2004). These techniques have been surveyed by Katić (Katić & Vukobratović, 2005). As the ZMP control is non-linear an SVR (Vapnik, 1998) is appropriate. SVR calculates the optimal hyper plane for the training data and works faster than several other computational intelligence techniques (Ferreira et al., 2007a).

In this work the training of the SVR uses values obtained by simulating the full dynamic model of the biped robot. Some walking experiments were conducted to test the implemented control algorithm. The robot was subjected to external sagittal pushing forces and the dragging of masses. The experiments were performed with and without the SVR controller active and the results show the effectiveness of the SVR controller together with the presented gait, based on the human locomotion.

## 2. Implemented robot and software

A biped robot was designed and built at the Institute of System and Robotics of the Department of Electrical and Computer Engineering of the University of Coimbra, in Portugal. The mechanical structure of the robot shown in Fig. 1 has the main joints of hip, knee, and ankle, for each leg. There is another joint, an active inverted pendulum that is

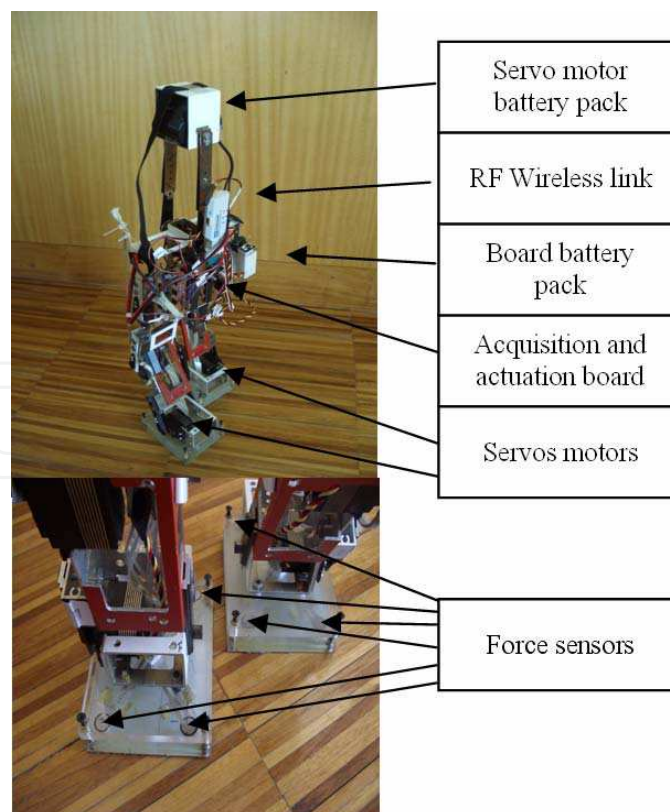


Fig. 1. Implemented robot.

used for the lateral balance of the structure. The robot carries its battery pack on this inverted pendulum. The robot is actuated by seven servo motors and the structure is made of acrylic and aluminium. It weighs 2.3 kg and is 0.5 m tall.

The robot was designed to move in both horizontal and inclined planes, to go up and down stairs, and has a speed of approximately 0.05 m/s. A 9600 bit/s RS232 wireless transmission link binds the control software, that is running on a PC, to the robot. The robot board has two PIC microprocessors, one to acquire the digital values of the force sensors and the other to actuate the servo motors.

An integrated software platform was developed which allows both the simulation and the real time control of the biped robot. The software screen layout is illustrated in Fig. 2.

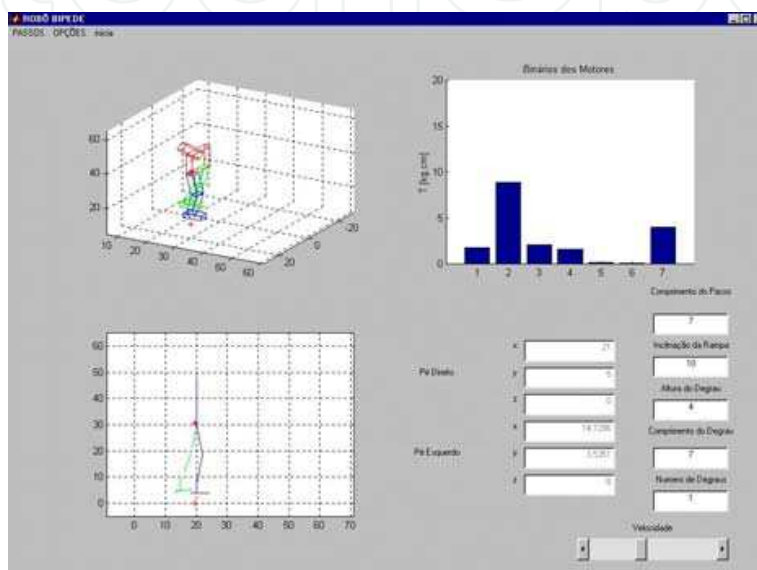


Fig. 2. Simulation and control software window.

Because it is very important to have very good mechanical contact between the force sensors (strip type) and the robot's feet, two different mechanical configurations were tested, as shown in Fig. 3. One of them uses a 9 mm of diameter cylinder (size of the active area of the sensor), and the other uses a semi-sphere to contact each sensor. Initially the cylindrical configuration was used and the signal was found to have a poor precision, due to the distribution of the force over the surface of the sensor. With the spherical configuration this problem was solved because the force is applied at a single point.

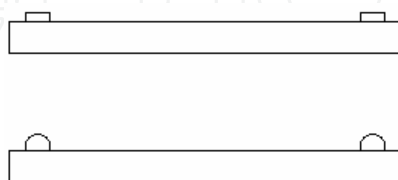


Fig. 3. Detail of the mechanical configurations used to improve the contact of the robot's feet with the force sensors.

### 3. Robot's 3D model and dynamics

Kinematics allows the movement of a robot to be described in terms of its position, speed and acceleration. Kinematics ignores the concepts of force, mass and inertia. The most

widely-used representation is the Denavit-Hartenberg formalism. The systems of axes adopted to model the biped robot are shown in Fig. 4, together with a 3D model of the robot.

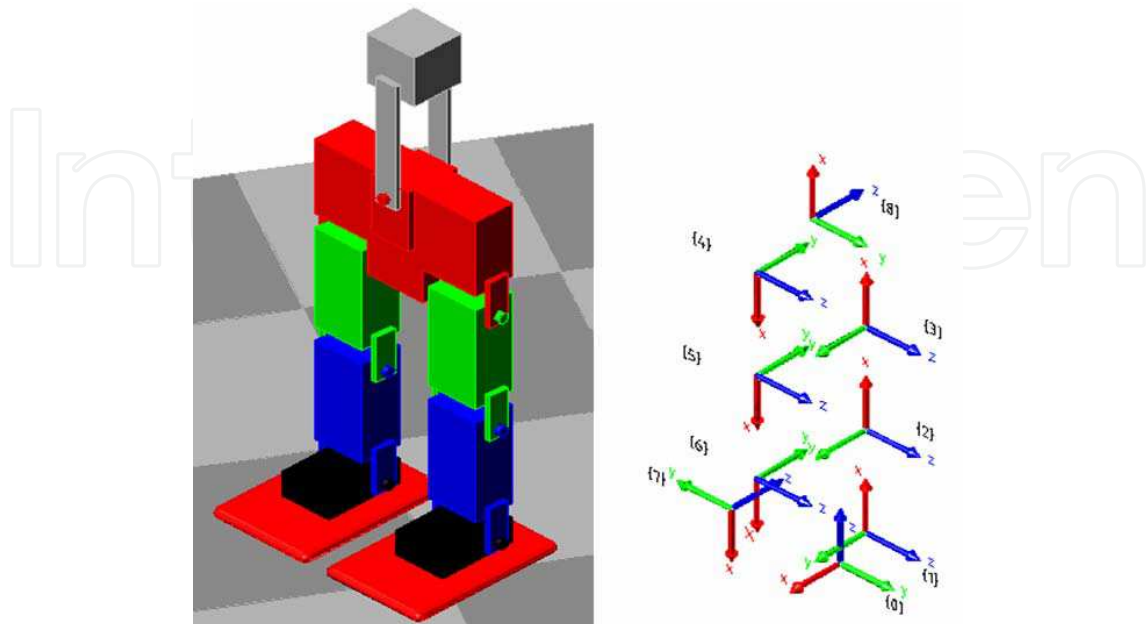


Fig. 4. 3D model and the respective coordinate systems.

Dynamics is the field of physics that studies the application of systems of forces and moments to a rigid body. In the case of the biped robot the ZMP formulation can be used (Hang et al., 1999), based on a dynamic calculation.

For a robot with four or more legs it is possible to consider the static stability that uses the center of gravity, but for a biped robot the dynamic stability may have to be taken into account, and the calculation of the ZMP makes this possible. The ZMP is defined as the point on the ground where the sum of all the active moments of force is null. In Fig. 5, the minimum distance between the ZMP and the border of the stable region is called the stability margin, and this can be considered as an indicator of the quality of the robot's stability.

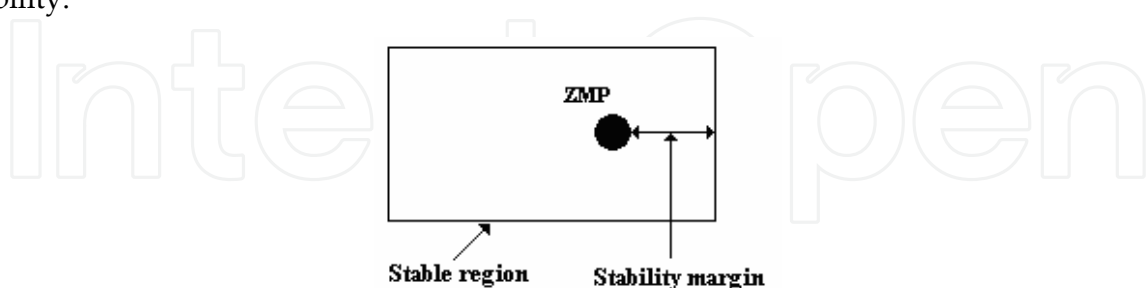


Fig. 5. Definition of the stability margin.

If the ZMP is inside the polygon of contact (stable region of the foot) between the foot and the ground, it can be said that the biped robot is stable. When the distance between the ZMP and the border of the stable region of the foot is the greatest, that is, when the coordinates of the ZMP are next to the center of the stable region, it can be said that the biped robot exhibits a high stability. For the robot model in Fig. 6, with the physical characteristics presented in Table I, the ZMP location is calculated by

$$X_{zmp} = \frac{\sum_{i=0}^7 m_i (\ddot{z}_i + g) x_i - \sum_{i=0}^7 m_i \ddot{x}_i z_i - \sum_{i=0}^7 I_{iy} \alpha_{iy}}{\sum_{i=0}^7 m_i (\ddot{z}_i + g)} \quad (1)$$

$$Y_{zmp} = \frac{\sum_{i=0}^7 m_i (\ddot{z}_i + g) y_i - \sum_{i=0}^7 m_i \ddot{y}_i z_i + \sum_{i=0}^7 I_{ix} \alpha_{ix}}{\sum_{i=0}^7 m_i (\ddot{z}_i + g)} \quad (2)$$

where  $\ddot{x}$ ,  $\ddot{y}$  and  $\ddot{z}$  are linear accelerations,  $I_{ix}$  and  $I_{iy}$ , are inertia coefficients,  $\alpha_{ix}$  and  $\alpha_{iy}$  are angular accelerations,  $m_i$  is the mass of the link  $i$ , and  $g$  is the gravitational acceleration. The aim of this work is the control of the robot in the sagittal plane. The control variable is the  $X_{zmp}$ . The lateral control is assured by the pendulum movement and is not studied here.

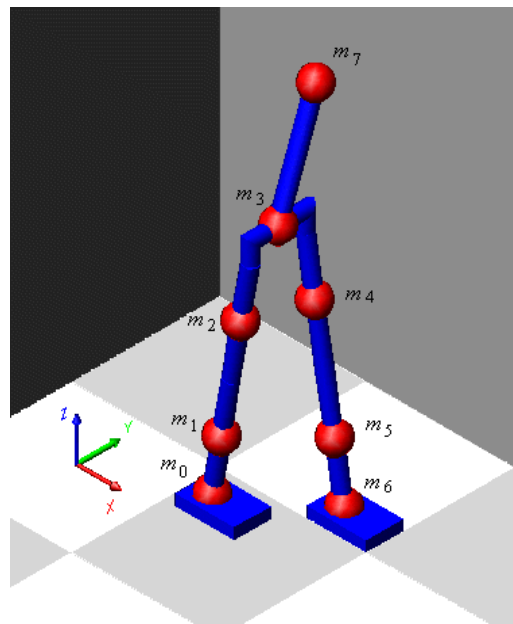


Fig. 6. Biped lumped mass model.

Biped	Mass (kg)	Length (m)	$I_x$ ( $\times 10^{-4}$ kg.m <sup>2</sup> )	$I_y$ ( $\times 10^{-4}$ kg.m <sup>2</sup> )
Foot	0.28x2	0.035	2.64	3.51
Shank	0.15x2	0.115	7.23	6.81
Thigh	0.15x2	0.115	7.23	6.81
Haunches	0.60	0.065	21.25	9.70
Pendulum	0.54	0.170	159.58	160.17

Table 1. Physical characteristics of the biped robot.

#### 4. Designed gaits

A gait has been chosen that was conceived with the goal of being similar to human locomotion in horizontal planes. To describe a robotic human-like gait only the hip and ankle trajectories are needed. The knee trajectory depends on these two trajectories.

Humans are among the best biped walkers, which is a good reason for obtaining their joint trajectories when they walk, and then applying this information to a biped robot, even though its physical characteristics differ from those of a human being.

The joint trajectories of hip, knee and ankle in the sagittal plane during a single gait cycle of a normal human being have been presented by Winter (Winter, 1990).

To acquire human trajectories an acquisition system was developed (Ferreira et al., 2007b). Images were captured with a color webcam that has the following characteristics: CMOS 640 × 480 (VGA) sensor, maximum of 30 frames per second, USB 2 interface. Trajectory data were obtained with a 26 year-old male, 1.85 m tall. Several light emitting diodes (LED) were placed on strategic points on the male (Fig. 7a). Fig. 7b shows the model used to calculate the joint angles, where H is the point on the heel, T is the tip of the foot, K is the point on the knee, HI is the point on the hip and SH is the point on the shoulder. These reference points were captured by placing the camera perpendicular to the background, 3 m away from it and 0.75 m from the floor. This latter distance is half the distance from the floor to the highest reference point, which is the shoulder mark.

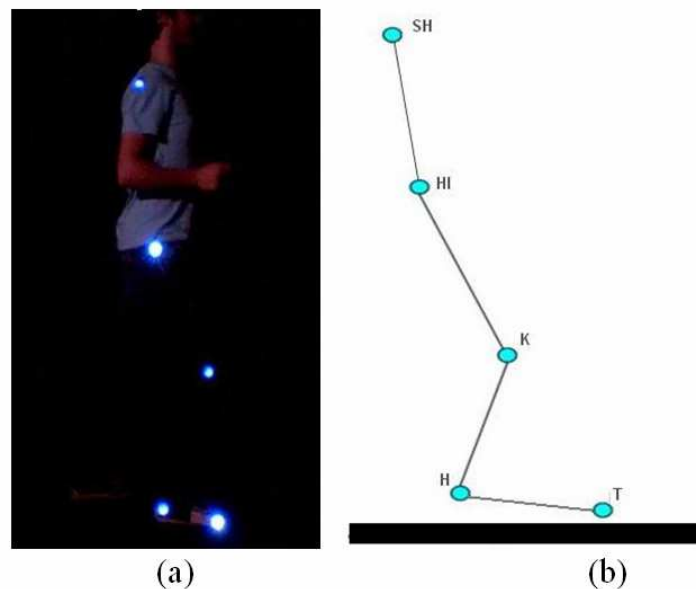


Fig. 7. (a) White light LED used as reference points on the person and (b) reference points on the person's model.

After the image acquisition of the reference points, the coordinates of the mass centers of these reference points were calculated for each frame and their trajectories obtained. The next step was to normalize the points of the trajectories and obtain a polynomial regression (which has square coefficient relation 0.996). This can be applied to any robot, using the height of the leg ( $Z_L$ ) and the step length ( $X_S$ ) as scale factors. So the hip and ankle trajectories are calculated by (3) and (4).

$$\begin{bmatrix} X_{hip} \\ Z_{hip} \\ X_{ankle} \\ Z_{ankle} \end{bmatrix}_{mov}^T = (A \cdot G_{mov})^T \cdot XZ_{mov} \quad (3)$$

$$\begin{bmatrix} X_{hip} \\ Z_{hip} \\ X_{ankle} \\ Z_{ankle} \end{bmatrix}_{gnd}^T = (A \cdot G_{gnd})^T \cdot XZ_{gnd} \quad (4)$$

where

$$A = \begin{bmatrix} 0 & 0 & 0 & 0 & 10.263E-03 & 249.033E-03 \\ 0 & 0 & 0 & -158.826E-06 & 78.736E-04 & 897.685E-03 \\ 0 & 0 & -15.67E-06 & 121.278E-05 & -14.623E-04 & 26.52E-04 \\ -180.869E-10 & 208.426E-08 & -745.788E-07 & 585.999E-06 & 954.539E-05 & -250.062E-06 \end{bmatrix}$$

is a coefficient polynomial matrix,

$$G_{mov} = \begin{bmatrix} (S_{\%} - 50)^5 \\ (S_{\%} - 50)^4 \\ (S_{\%} - 50)^3 \\ (S_{\%} - 50)^2 \\ (S_{\%} - 50) \\ 1 \end{bmatrix} \quad \text{and} \quad XZ_{mov} = \begin{bmatrix} X_S & 0 & 0 & 0 \\ 0 & Z_L & 0 & 0 \\ 0 & 0 & X_S & 0 \\ 0 & 0 & 0 & Z_L \end{bmatrix}$$

are the percentage of the stride cycle for the moving foot and a scale factor, respectively,

$$G_{gnd} = \begin{bmatrix} S_{\%}^5 \\ S_{\%}^4 \\ S_{\%}^3 \\ S_{\%}^2 \\ S_{\%} \\ 1 \end{bmatrix} \quad \text{and} \quad XZ_{gnd} = \begin{bmatrix} X_S & 0 & 0 & 0 \\ 0 & Z_L & 0 & 0 \\ 0 & 0 & 0 & 0 \\ 0 & 0 & 0 & 0 \end{bmatrix}$$

are the percentage of the stride cycle for the grounded foot and a scale factor, respectively.

The values of the parameters used in the experiment were  $X_S = 0.23$  m and  $Z_L = 0.07$  m. The trajectories obtained for the hip and the ankle are shown in Fig. 8 for the grounded foot, and in Fig. 9 for the moving foot. The torso angle in the human walk is similar to a cosine function.

## 5. Trajectory planning algorithm

The control method used in this work to achieve the sagittal equilibrium of the robot consists of correcting the hip and pendulum angle (torso angle) in order to keep the ZMP in the center of the grounded foot (with a tolerance of 4 mm).

We describe next the torso trajectory planning algorithm. It was executed off-line, and the result was used for the SVR training and for the amplitude setting of the initial predictive trajectory of the torso. First, taking into account the gait's characteristics, several via points

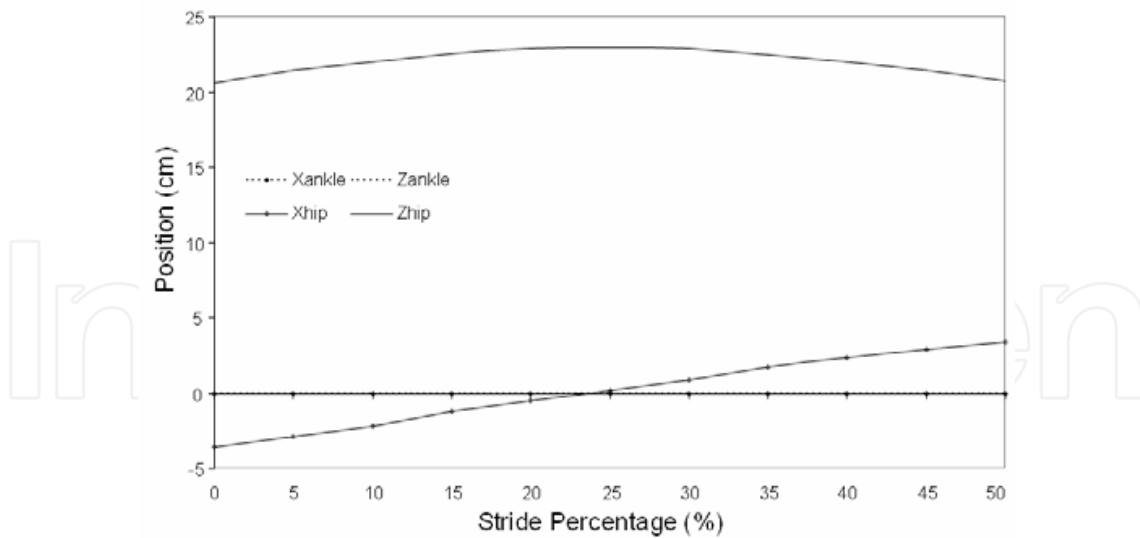


Fig. 8. Trajectories of the hip and ankle for the grounded foot.

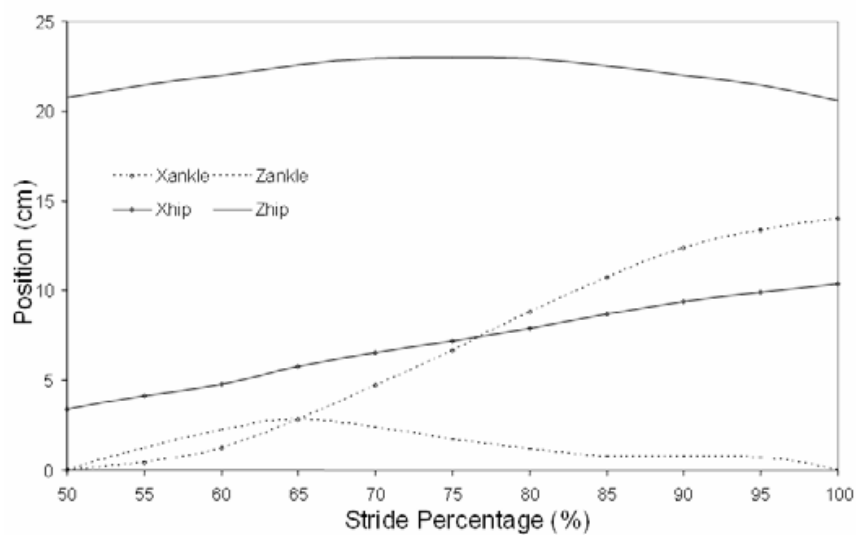


Fig. 9. Trajectories of the hip and ankle for the moving foot.

of the trajectory are obtained, and the trajectory of the foot is generated using a cubic spline. After that, the trajectories of the joints are calculated using direct and inverse kinematics; finally, the ZMP is calculated and the stability margin determined. This stability margin is then used to make iterative corrections to the torso angle, using the desired ZMP (center of the grounded foot) as reference. This procedure is repeated for all frames of the step.

It must be noticed that some gaits may not be stable because the working range of the servo motors used is limited. Fig. 10 shows the algorithm explained before.

This algorithm is used for the static and dynamic models, but the spline is not needed in the static model, which greatly reduces computational effort. The dynamic model requires four splines for each link, resulting in a great computational effort and making real-time computation difficult.

Fig. 11 shows the ZMP trajectory obtained with the previous algorithm for the “walking in horizontal planes” gait with a step length of 0.11 m. The figure shows ZMP points marked with crosses.

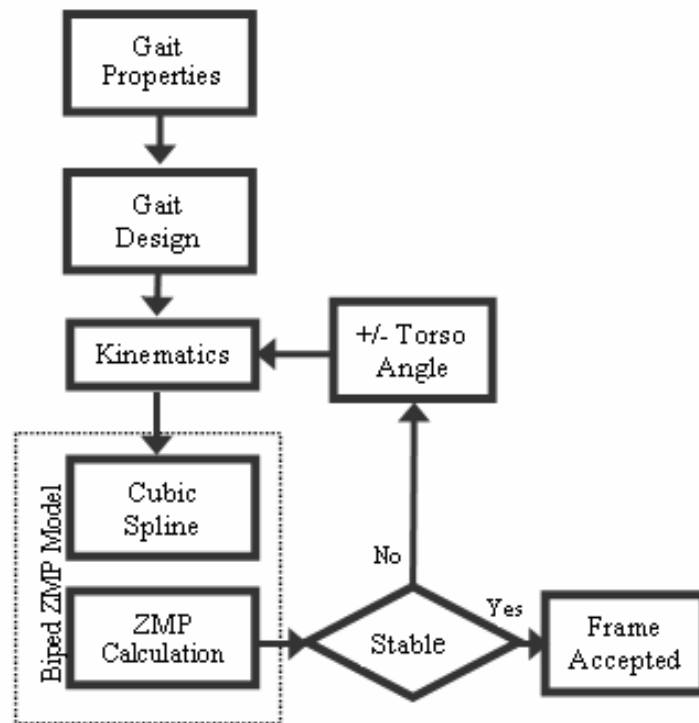


Fig. 10. Trajectory planning algorithm.

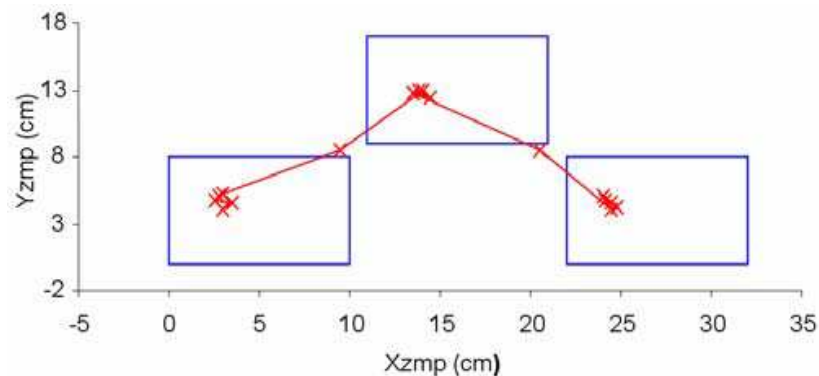


Fig. 11. ZMP Trajectory.

The SVR training data are the  $\Delta\theta_{\text{Torso}}$  (torso angle correction), the  $X_{\text{ZMP}}$  and  $DX_{\text{ZMP}}$  ( $X_{\text{ZMP}}$  discrete time derivative). The  $\Delta\theta_{\text{Torso}}$  versus  $DX_{\text{ZMP}}$  data were obtained by expert knowledge having a PD controller in mind. The  $\Delta\theta_{\text{Torso}}$  versus  $X_{\text{ZMP}}$  training data were obtained by simulation using the trajectory planning algorithm, described above, for several step lengths and times. The result of the simulation was the relation  $K(t)$  between the required torso angle correction ( $\Delta\theta_{\text{Torso}}$ ) and the difference between the actual  $X_{\text{ZMP}}$  and the desired  $X_{\text{ZMP}}$  ( $X_{\text{ZMPD}}$ , which is zero because it is at the origin of the coordinate system), to maximize the biped robot stability margin, as a function of the step time  $T_{\text{step}}$  (see Fig. 12).

Analyzing Fig. 12, it can be considered that  $K$  does not depend on the length of the gait, but only on the step time. Using a curve fitting algorithm, the expression

$$K(t) = 0.002 \cdot t^4 - 0.0637 \cdot t^3 + 0.7795 \cdot t^2 - 4.4803 \cdot t + 2.7866 \quad (5)$$

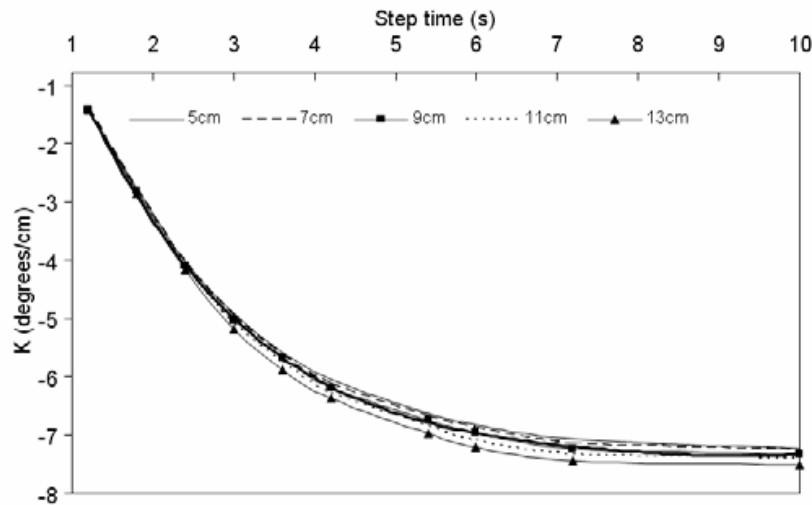


Fig. 12. The relation  $K = \Delta\theta_{\text{Torso}} / (X_{\text{ZMP}} - X_{\text{ZMPD}})$ .

was obtained. With this relationship the static model can be used to generate a first estimate for  $\theta_{\text{torso}}$ , using the center of gravity (CoG), instead of the  $X_{\text{ZMP}}$ .

It was found that the human torso angle trajectory is similar to a cosine function. The predicted torso angle is then given by

$$\theta_{\text{torso}} = A \cdot \cos\left(\frac{2\pi \cdot S\%}{100}\right) \quad (6)$$

where  $A = X_{\text{CoG}} \cdot K(T_{\text{Step}})$  and  $S\%$  is the gait time percentage. The value of  $X_{\text{CoG}}$  ( $X$  coordinate of the center of gravity of the robot) is calculated in the transition from the double phase to the single phase using

$$X_{\text{CoG}} = \frac{\sum_{i=0}^7 m_i \cdot g \cdot x_i}{\sum_{i=0}^7 m_i \cdot g} \quad (7)$$

where  $m_i$  is the mass of the link  $i$  and  $g$  is the gravitational acceleration.

## 6. Control strategy

The proposed biped control model is shown in Fig. 13. The joint angles of the robot, except the torso angle, are determined by inverse kinematics using the designed gait (3) and (4) for the entire step. The values of the torso angle are predicted by (6). After that, for each frame, all joint angles values are sent to the biped robot and the real  $X_{\text{ZMP}}$  ( $X_{\text{ZMPR}}$ ) is determined reading the force sensors placed under its feet. The  $X_{\text{ZMPR}}$  value is then used by the SVR to correct the torso angle in real time. The output of the SVR is an increment to be added to the torso angle given by (6).

This control strategy assures the stability of the robot, even if external disturbances occur. In order to allow real time control, the actual (real) value of the ZMP (ZMPR) is needed. When the ZMP is within the stable area, the ZMP and the centre of pressure (CoP) are the same. To determine the CoP, four force sensors are used in each foot of the robot, as Fig. 14

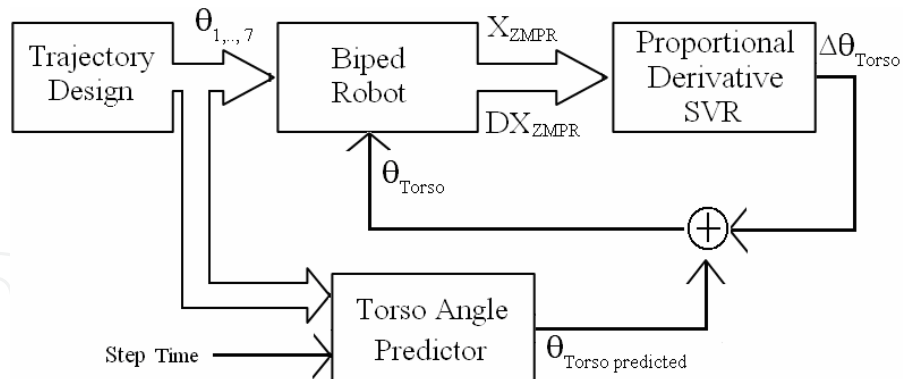


Fig. 13. SVR control of the biped robot.

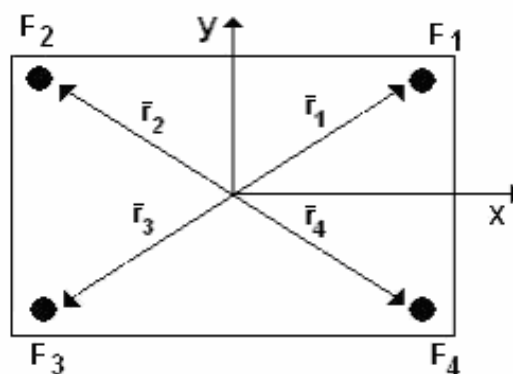


Fig. 14. Top view diagram of the foot, showing the location of the force sensors.

shows. These sensors are used to detect the force intensity and where the force is exerted, which is determined by

$$CoP = \frac{\sum_{i=1}^8 F_i \cdot \bar{r}_i}{\sum_{i=1}^8 F_i} \tag{8}$$

where  $F_i$  is the force measured in sensor  $i$ , and  $\bar{r}_i$  is the sensor  $i$  position vector. Force sensor signals are acquired by an analog to digital converter (ADC) with 10-bit resolution and with a maximum of 30 Hz sampling rate. The force measurements are noisy and the force sensor is sensitive to vibrations during the motion, so a second order Butterworth low pass filter is used to remove noise and high frequency vibrations from the force sensor signal. The difference equation for a second-order low-pass Butterworth digital filter has the form

$$y_k = b_1x_k + b_2x_{k-1} + b_3x_{k-2} - a_2y_{k-1} - a_3y_{k-2} \tag{9}$$

where  $y$  is the filtered variable,  $x$  is the unfiltered variable,  $x_k$  is the value of  $x$  at time  $t_k$ ,  $y_k$  is the value of  $y$  at time  $t_k$ ,  $t_k = k \cdot T$  is the current time,  $T = t_k - t_{k-1}$  is the constant sampling interval, and  $k$  is an integer.

## 7. Support vector machines

Support Vector Machines (SVM) were developed by Vapnik (Vapnik, 1998) first to solve classification problems, and then they were successfully extended to regression and density estimation problems (Mohamed & Farag, 2003). SVM have gained popularity due to their many attractive features and promising empirical performance. The formulation of SVM employs the Structural Risk Minimization (SRM) principle, which has been shown to be superior to the traditional Empirical Risk Minimization (ERM) principle employed in the other non-parametric learning algorithms (e.g. neural networks) (Vapnik et al., 1999). SRM minimizes an upper bound on the generalization error as opposed to ERM, which minimizes the error on the training data. This difference makes SVM more attractive in statistical learning applications. SVM are used for classification and regression. In this work an SVM is used for regression, being usually designated by SVR.

### 7.1 Support Vector Regression (SVR)

Given a set of data points,  $\{(x_1, z_1), \dots, (x_l, z_l)\}$ , such that  $x_i \in \mathbb{R}^n$  is an input and  $z_i \in \mathbb{R}$  is a target output, the standard form of support vector regression (Vapnik, 1998) is:

$$\begin{aligned} \min_{w, b, \xi, \xi^*} \quad & \frac{1}{2} w^T w + C \sum_{i=1}^l \xi_i + C \sum_{i=1}^l \xi_i^* & (10) \\ \text{subject to} \quad & w^T \phi(x_i) + b - z_i \leq \varepsilon + \xi_i, \\ & z_i - w^T \phi(x_i) - b \leq \varepsilon + \xi_i^*, \\ & \xi_i, \xi_i^* \geq 0, \quad i = 1, \dots, l. \end{aligned}$$

For practical reasons, instead of solving this minimization problem its dual form, more manageable, is used:

$$\begin{aligned} \min_{\alpha, \alpha^*} \quad & \frac{1}{2} (\alpha - \alpha^*)^T Q (\alpha - \alpha^*) + \varepsilon \sum_{i=1}^l (\alpha_i + \alpha_i^*) + \sum_{i=1}^l z_i (\alpha_i - \alpha_i^*) & (11) \\ \text{subject to} \quad & \sum_{i=1}^l z_i (\alpha_i - \alpha_i^*) = 0, \quad 0 \leq \alpha_i, \alpha_i^* \leq C, \quad i = 1, \dots, l, \end{aligned}$$

where  $Q_{ij} = k(x_i, x_j) \equiv \phi(x_i)^T \phi(x_j)$ .

The approximate function is

$$f(x) = \sum_{i=1}^l (-\alpha_i + \alpha_i^*) k(x_i, x) + b \quad (12)$$

For the biped robot controller we used the Gaussian kernel

$$k(x_i, x_j) = \exp(-\gamma | |x_i - x_j| |^2) = \exp\left(-\frac{(x_i - x_j)^2}{2\sigma^2}\right) \quad (13)$$

since it demonstrated to perform well on this problem.

Fig. 15 shows the insensitive band (tube) of a typical non-linear regression function when the SVR method is used. To solve the SVR with this kernel, the LIBSVM (Chang & Lin, 2007) was used, where the  $C$ ,  $\epsilon$  and  $\gamma$  parameters of (10) and (13) must be chosen to generate the best final model, for this training data. Parameter  $C$  represents the importance of the values outside the regression tube,  $\epsilon$  corresponds to the *radius* of the regression function tube and  $\gamma$  represents the Gaussian kernel width. Therefore, the number of support vectors is a decreasing function of  $\epsilon$  and a nonzero value of  $\epsilon$  is required to avoid overfitting. On the other hand, a too large value of  $\epsilon$  could result in an underfitting.

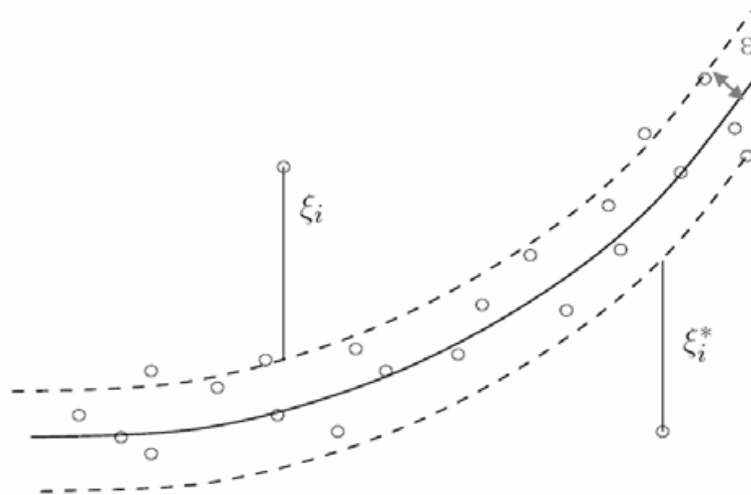


Fig. 15. The insensitive band for a non-linear regression function.

## 7.2 Support Vector Regression simulation

In this work the SVR was trained with 239 normalized data points and tested with another 68 data point, as defined in Section 5. To choose the above parameters,  $\epsilon$  was varied from 0.01 to 0.2 with increments of 0.01,  $C$  was varied from 0.1 to 2 with increments of 0.1 and  $\gamma$  was varied from 1 to 4 with increments of 0.1. Fig. 16 plots the minimum MSE (mean square

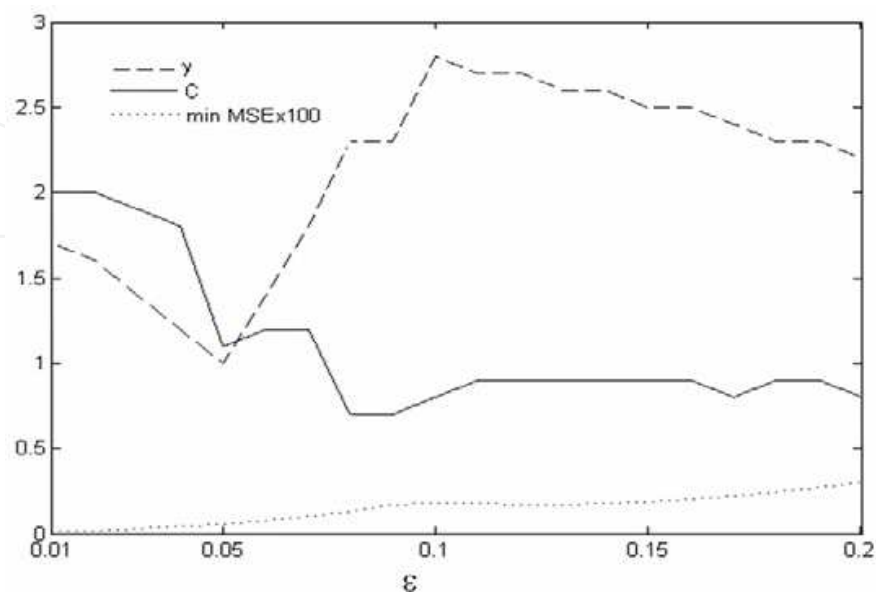


Fig. 16.  $\gamma$ ,  $C$  and MSE versus  $\epsilon$ .

error) for the combinations defined above, as well as the corresponding  $C$  and  $\gamma$  parameters, as functions of  $\varepsilon$ .

Analyzing Fig. 16, the value of  $\varepsilon = 0.13$  was chosen because it corresponds to the highest point of the region where the MSE is constant and small. For this value of  $\varepsilon$  the other parameters are  $\gamma = 2.6$  and  $C = 0.9$ . To complement the performances of the SVR, Fig. 17 and 18 show the variation of the mean square error (MSE) and the mean absolute error (MAE) versus  $C$  and  $\gamma$  respectively. The average time to calculate the SVR was 0.2 ms, which proved to be adequate for our problem. Fig. 19 shows the behavior of the final model.

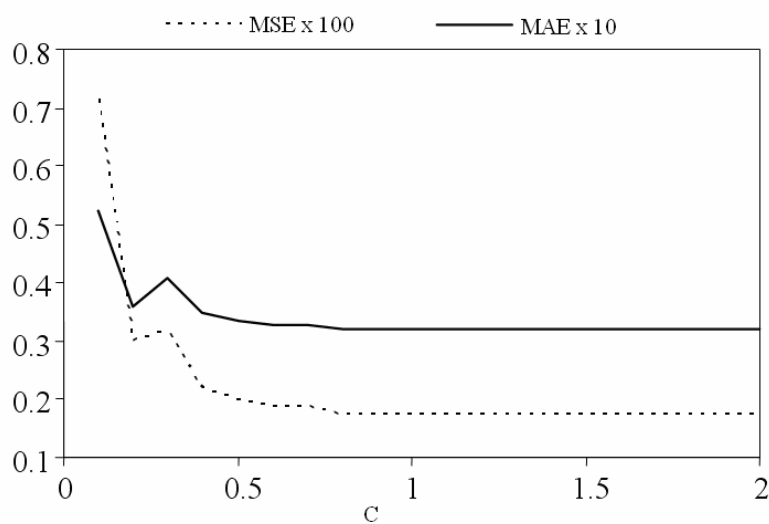


Fig. 17. MSE and MAE against  $C$ .

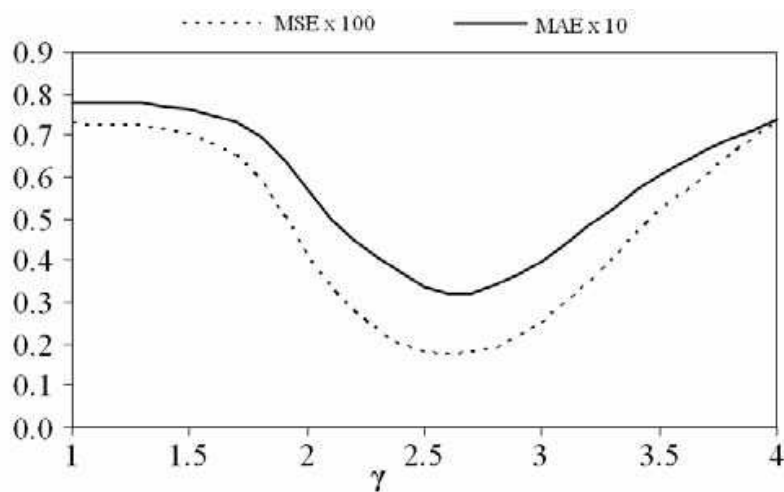


Fig. 18. MSE and MAE against  $\gamma$ .

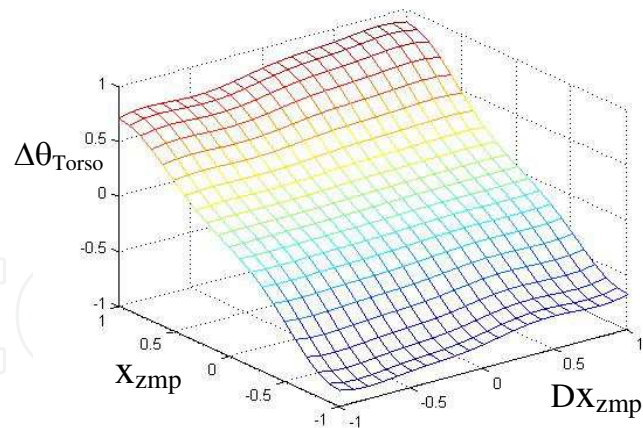


Fig. 19. Behavior of the final model.

## 8. Experimental results

To determine the functionality of the balance control system based on an SVR, several experiments were performed. With this control technique, the stability of the robot is assured, even in the event of external disturbances.

The values presented in the next figures were normalized such that unit values correspond to 25 degrees for  $\theta_{\text{torso}}$ , 10 degrees for  $\theta_{\text{ankle}}$ , 55 degrees for the pendulum lateral angle ( $\theta_{\text{lateral}}$ ), 0.047 m for  $X_{\text{ZMP}}$  and by 9.8 N for the external force.

In the first experiment the biped robot was walking on a flat surface, playing back the human leg trajectories obtained with the video camera, without the SVR controller active. The torso was kept vertical. The  $X_{\text{zmp}}$  behavior is shown in Fig. 20 and it can be seen that it is very irregular, and that after some steps the robot falls. The origin of the  $X_{\text{zmp}}$  axes corresponds to the center of the support area.

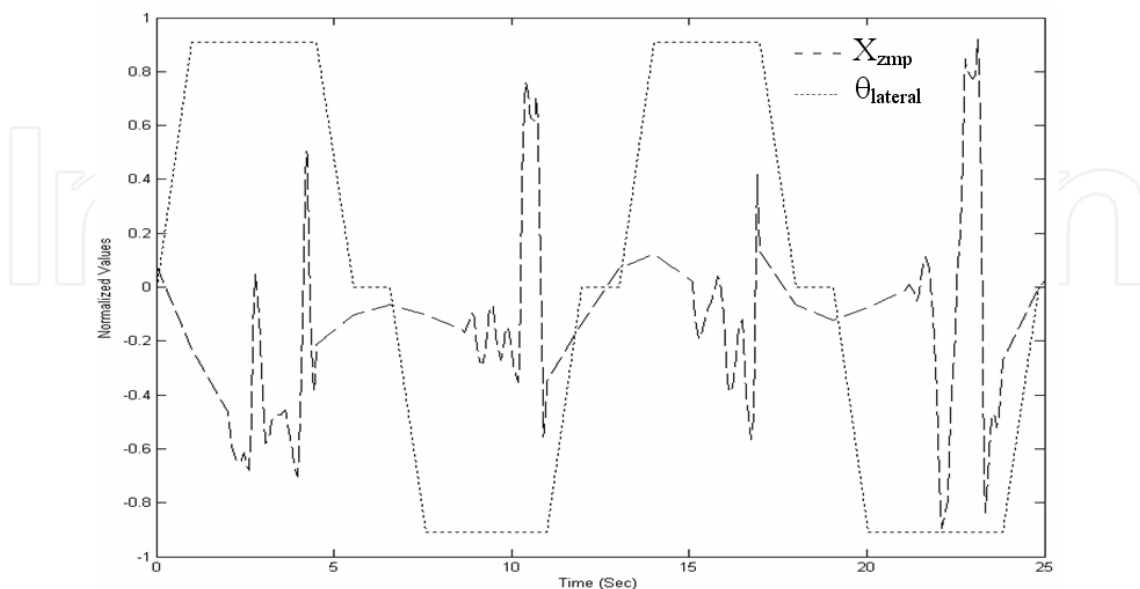


Fig. 20.  $\theta_{\text{Lateral}}$  and  $X_{\text{zmp}}$  obtained with the robot walking on a flat surface and the torso always vertical, without the SVR controller active.

In the second experiment the robot was walking on a flat surface with the SVR controller active. In this case both the  $X_{zmp}$  and the torso angle exhibit regular behavior (see Fig. 21). A walking snapshots of one step is shown in Fig. 22. At the end of this experiment an external force was applied, pushing the robot on the back. The force was applied at a height of 0.3 m, and the robot maintained its stability, as can be seen in Fig. 23.

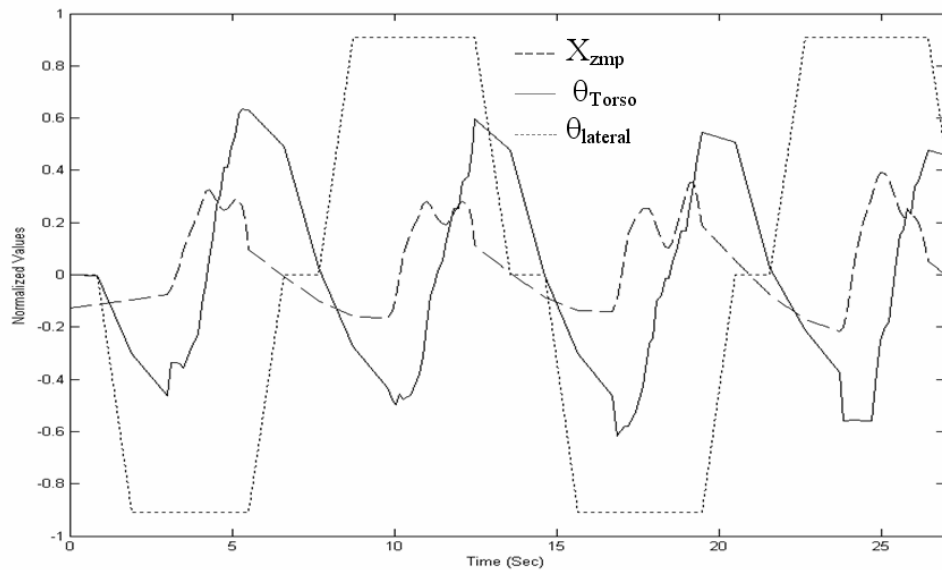


Fig. 21.  $\theta_{Lateral}$ ,  $\theta_{Torso}$  and  $X_{zmp}$  obtained with the robot walking on a flat surface and the torso control active.

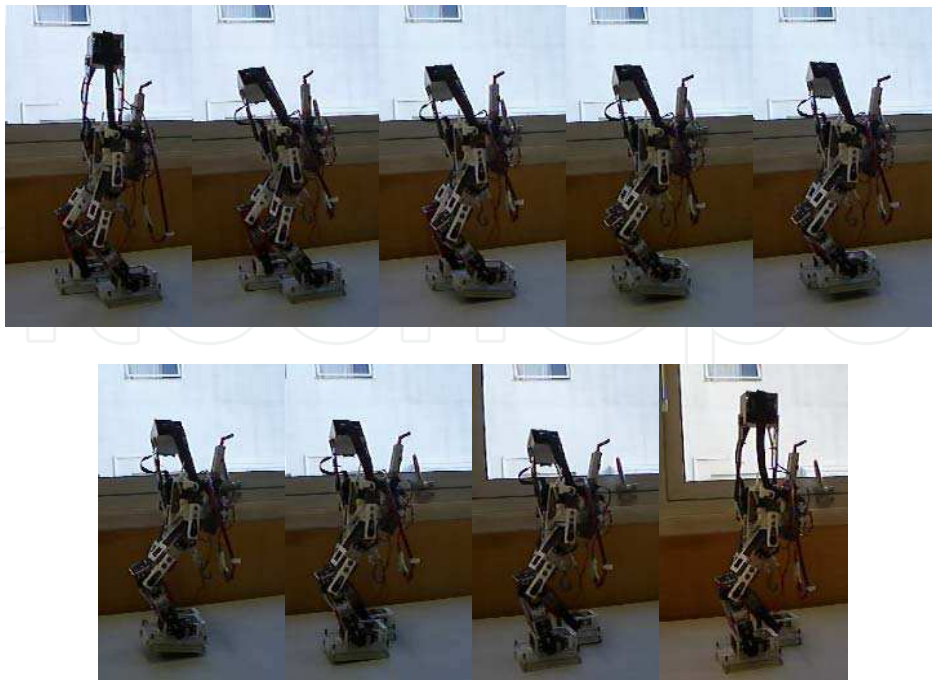


Fig. 22. Walking snapshots on a flat surface and the torso control active.

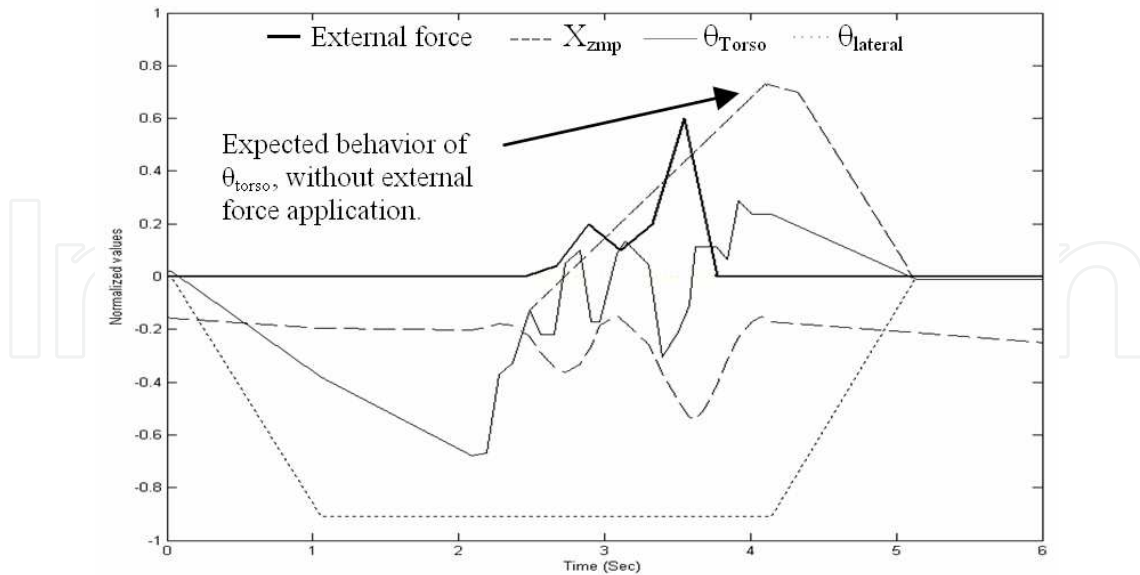


Fig. 23.  $\theta_{\text{Lateral}}$ ,  $\theta_{\text{Torso}}$  and  $X_{\text{zmp}}$  obtained with the robot walking on a flat surface and the torso control active, and under an external force.

In the third experiment an external pushing force was applied on the rear side of the robot when it was standing with only one foot on the ground. As can be seen in Fig. 24 and in the snapshots shown in Fig. 25, when the force is applied the controller maintains the stability. In the final experiment the robot suffers another external pushing force (greater than the force applied in the third experiment and for a little longer) applied on its front side. As shown in Fig. 26 and Fig. 27 the controller is able to stabilize the robot.

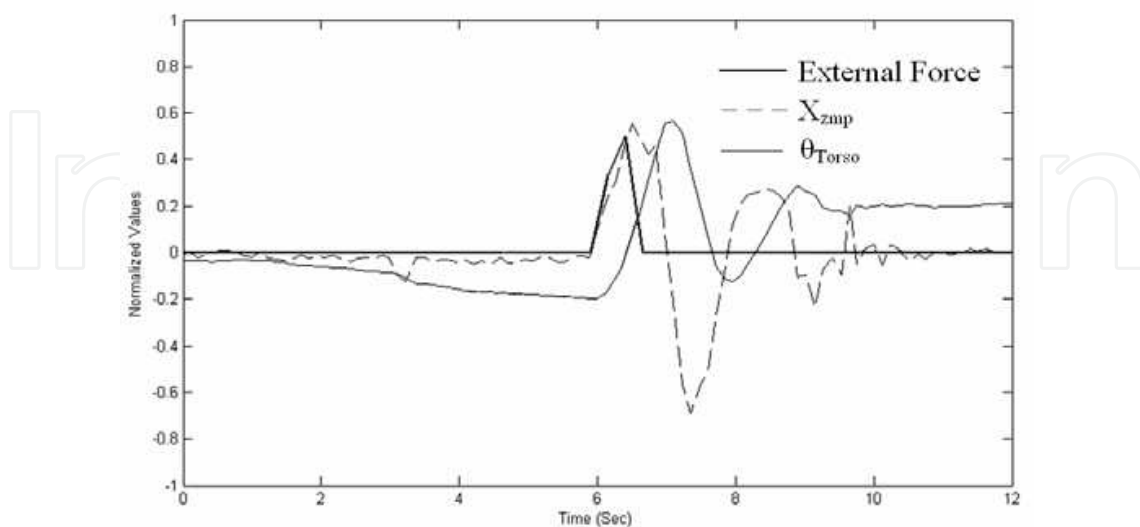


Fig. 24.  $\theta_{\text{Torso}}$  and  $X_{\text{zmp}}$  obtained when the robot is pushed from behind, standing with only one foot on the ground.

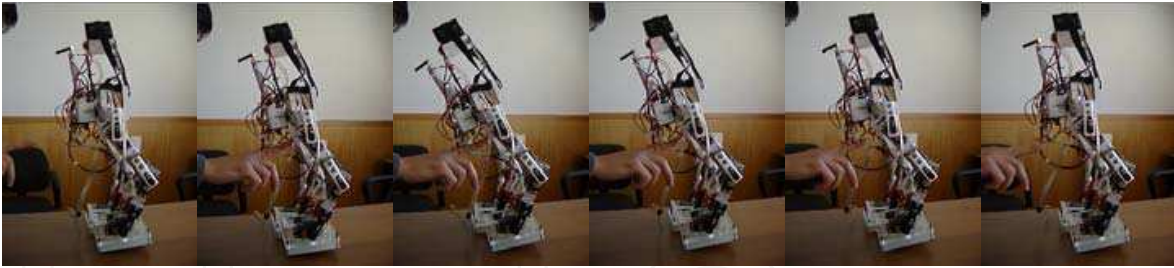


Fig. 25. Snapshots of a rear push.

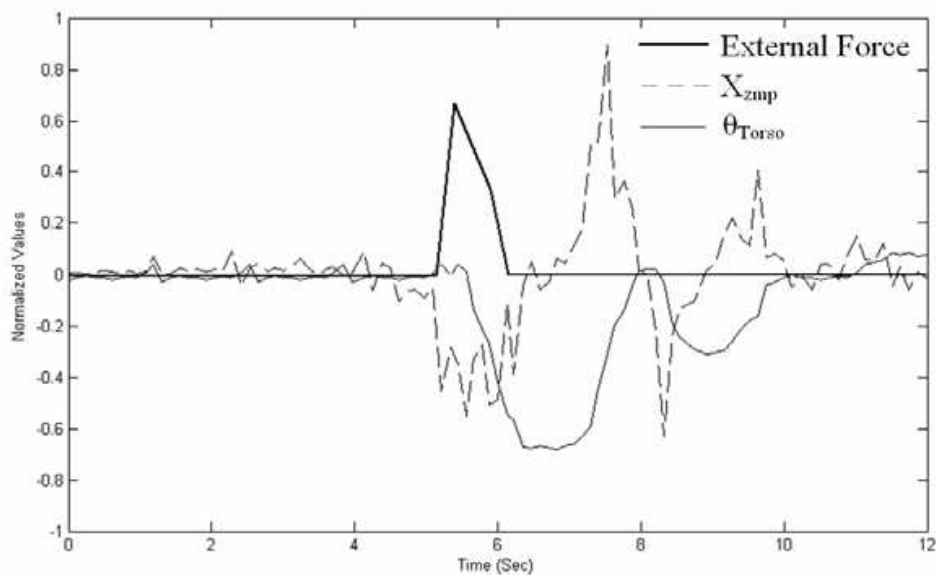


Fig. 26.  $\theta_{\text{Torso}}$  and  $X_{\text{zmp}}$  obtained when the robot is pushed from the front, standing with only one foot on the ground.

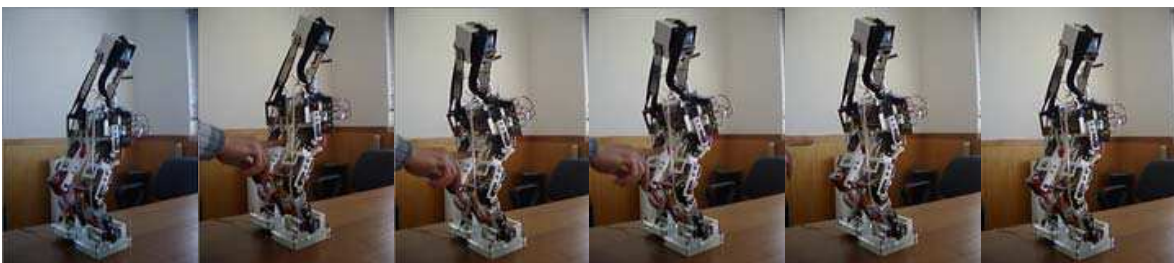


Fig. 27. Snapshots of a front push.

In these two next experiments the robot was walking on a flat surface, with a step length of 0.07 m, using the trajectories of the human gait, dragging a mass of 1.5 kg (that provides a pulling force of about 5 N), with (Fig. 28 and 29) and without (Fig. 30 and 31) the SVR controller active.

It is visible in Fig. 29 (with the SVR balance controller active) that the robot is able to pull the mass along the step, i.e., the mass moves forward 0.07 m (the step length), while in Fig. 31 (without the SVR balance controller active) the mass moves forward only 0.035 m and the robot falls in the next step. In Fig. 30 it is possible to see that the value of  $X_{\text{ZMP}}$  is in the limit of the stable area.

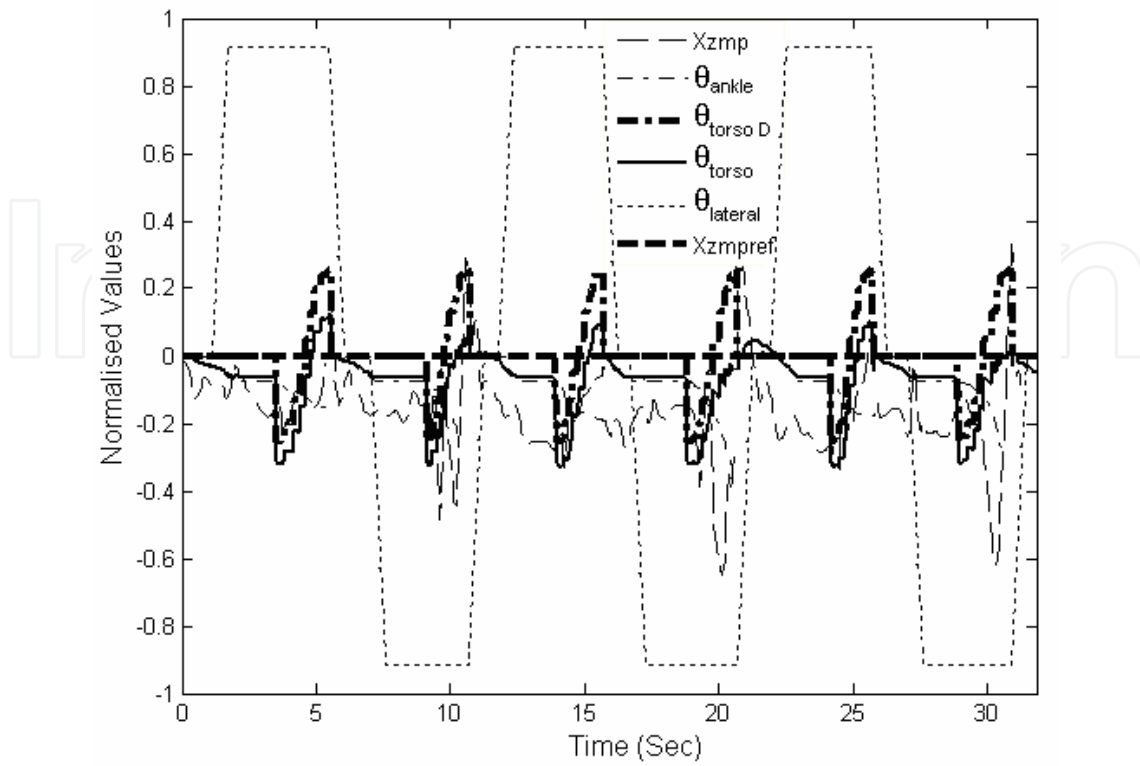


Fig. 28.  $X_{ZMP}$ ,  $X_{ZMPref}$ , ankle, designed torso ( $\theta_{torsoD}$ ), torso and lateral angles on a horizontal flat surface pulling a mass with the SVR controller active.

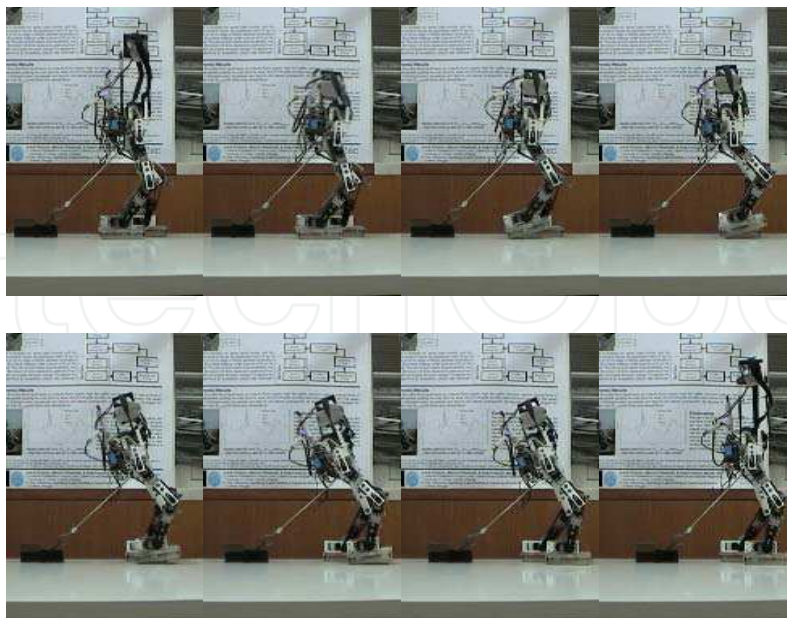


Fig. 29. Walking snapshots of one step on a horizontal flat surface pulling a mass with the SVR controller active.

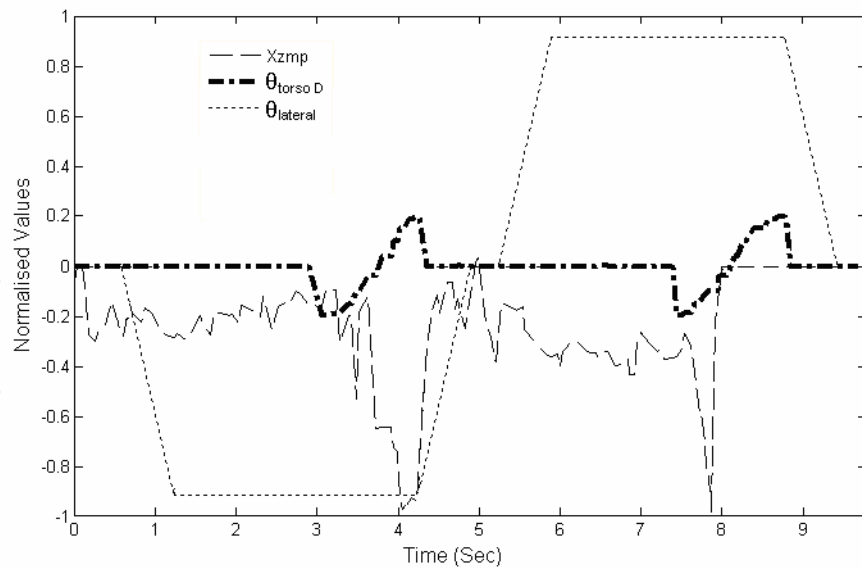


Fig. 30.  $X_{ZMP}$ , designed torso ( $\theta_{\text{torsoD}}$ ) and lateral angles on a horizontal flat surface pulling a mass without the SVR controller active.

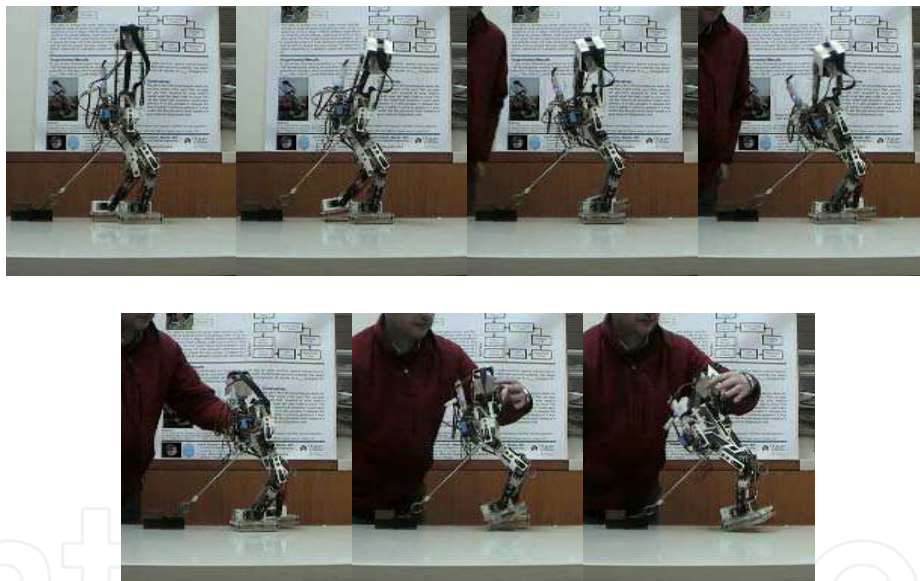


Fig. 31. Walking snapshots on a horizontal flat surface pulling a mass without the SVR controller active. The robot falls down at about  $t = 8\text{s}$ .

The effectiveness of the SVR controller is illustrated in Fig. 28 where the robot presents a good stability margin compared to Fig. 30 where the  $X_{ZMP}$  profile is irregular and the stability margin is close to zero at time about 4 seconds and zero at about 8 seconds, when the robot falls down.

## 9. Conclusions

The real time control of an 8-link biped robot using the dynamic model of the ZMP is difficult, due to the processing time of the corresponding equations. A simulator of an 8-link biped robot model was developed that allows training data to be obtained for an SVR. The

input variable  $DX_{zmp}$  was used to include the behavior of a PD controller in the SVR. The application of the SVR method requires a good trade off between over-fitting and under-fitting to obtain a smooth behavior for the final model.

The major advantage of the SVR is running in 0.2 ms which is 50 times faster than a neuro-fuzzy controller. The use of the SVR allows the real time control of the robot. This SVR uses the real CoP, acquired through force sensors placed under the robot's feet, as input. The SVR was tested and satisfactory results were obtained when the robot pulls a mass that is 65% of the robot's mass.

To obtain a good stable step it is very important to design good leg trajectories so that only a small variation of torso movement is needed to maintain balance. It was verified that the human-like gait is a good choice to use in this biped robot.

## 10. Acknowledgments

The authors would like to thank the Portuguese Fundação para a Ciência e a Tecnologia for financial support.

## 11. References

- Behnke, S. (2006). Online trajectory Generation for Omnidirectional Biped Walking, *Proc. of the 2006 IEEE International Conference on Robotics and Automation*, Orlando, Florida
- Chang, C. & Lin, C. (2007). LIBSVM: a Library for Support Vector Machines, January 2, 2007
- Chevallereau, C., Formal'sky, A. & Perrin, B. (1998). Low Energy Cost Reference Trajectories for a Biped Robot, *Proc. IEEE Int. Conf. Robotics and Automation*, pp. 1398-1404
- Choi, K. C., Lee, M. C. & Lee, J. M. (2006). Fuzzy Posture Control for a Biped Walking Robot Based on Force Sensor for ZMP, *The Eleventh International Symposium on Artificial Life and robotics*, Oita, Japan, January 23-25
- Ferreira, J. P., Amaral, T. G., Pires, V. F., Crisóstomo, M. M. & Coimbra A. P. (2004). A Neural-Fuzzy Walking Control of An Autonomous Biped Robot, *WAC - IEEE Conference*, Sevilha, 21-23
- Ferreira, J. P., Crisóstomo, M. M., Coimbra A. P. & Ribeiro, B. (2007a). Simulation control of a biped robot with Support Vector Regression, *IEEE International Symposium on Intelligent Signal Processing*, Madrid, Spain, 3-5 October
- Ferreira, J. P., Crisóstomo, M. M., Coimbra, A. P., Carnide, D. & Marto, A. (2007b). A Human Gait Analyzer, *IEEE International Symposium on Intelligent Signal Processing-WISP'2007*, Madrid, Spain, 3-5 October
- Jang, Y., Mark, S., Nixon & Chris, J. H. (2002). Extracting Human Gait Signatures by Body Segment Properties, *Fifth IEEE Southwest Symposium on Image Analysis and Interpretation*
- Hirai, K. M., Haikawa, Y. & Takenaka, T. (1998). The Development of Honda Humanoid Robot, *Proc. Int. Conf. Robotics and Automation*, pp. 1321-1326.
- Huang, Q., Kajita, S., Kaneko, K., Yokoi, K., Komoriya, K. & Tanie, K. (1999). A High Stability, Smooth Walking Pattern for a Biped Robot, *Proc. Int. Conf. Robotics and Automation*, pp. 65-71
- Katić, D. & Vukobratović, M. (2005). Survey of Intelligent Control Algorithms For Humanoid Robots, *Proceedings of the 16th IFAC World Congress*, July

- Mohamed, R. M. & Farag, A. A. (2003). Classification of Multispectral Data Using Support Vector Machines Approach for Density Estimation, *IEEE Seventh International Conference on Intelligent Engineering Systems, INES03, Assiut, Egypt, March 2003*
- Nakamura, M., Mori, M. & Nishii, J. (2004). Trajectory planning for a leg swing during human walking, *IEEE International Conference on Systems, Man and Cybernetics*
- Park, J. H. & Kim, K. D. (1998). Biped Robot Walking Using Gravity-Compensated Inverted Pendulum Mode and Computed Torque Control., *International Conference on Robotics and Automation*, volume 4, pp. 3528-3533
- Shin, C. L., Li, Y. Z., Churng, S., Lee, T. T. & Cruver, W. A. (1990). Trajectory Synthesis and Physical Admissibility for a Biped Robot During the Single-Support Phase, *Proc. Int. Conf. Robotics and Automation*, pp. 1646-1652
- Vapnik, V. (1998). *The Nature of Statistical Learning Theory*, Springer, New York
- Vapnik, V., Golowich, S. & Smola, A. (1999). Support Vector Method for Multivariate Density Estimation, *Advances in Neural Information Processing Systems*, Vol. 12, pp. 659-665, MIT Press, April 1999
- Vukobratovic, M. (1990). *Biped locomotion: Dynamics, Stability, Control and Application*, Berlin: Springer-Verlag
- Winter, D. A. (1990). *The Biomechanics and Motor Control of Human Movement*, 2nd Eds., John Wiley & Sons
- Zarrugh, M. Y. & Radcliffe, C. W. (1979). Computer Generation of Human Gait Kinematics, *J. of Biomechanics*, Vol. 12, pp. 99 - 111
- Zheng, Y. F. & Shen, J. (1990). Gait Synthesis for the SD-2 Biped Robot to Climb Sloping Surface, *IEEE Trans. on Robotics and Automation*, Vol. 6, No. 1, pp. 86-96

IntechOpen



## **Biped Robots**

Edited by Prof. Armando Carlos Pina Filho

ISBN 978-953-307-216-6

Hard cover, 322 pages

**Publisher** InTech

**Published online** 04, February, 2011

**Published in print edition** February, 2011

Biped robots represent a very interesting research subject, with several particularities and scope topics, such as: mechanical design, gait simulation, patterns generation, kinematics, dynamics, equilibrium, stability, kinds of control, adaptability, biomechanics, cybernetics, and rehabilitation technologies. We have diverse problems related to these topics, making the study of biped robots a very complex subject, and many times the results of researches are not totally satisfactory. However, with scientific and technological advances, based on theoretical and experimental works, many researchers have collaborated in the evolution of the biped robots design, looking for to develop autonomous systems, as well as to help in rehabilitation technologies of human beings. Thus, this book intends to present some works related to the study of biped robots, developed by researchers worldwide.

### **How to reference**

In order to correctly reference this scholarly work, feel free to copy and paste the following:

João P. Ferreira, Manuel Crisóstomo, A. Paulo Coimbra and Bernardete Ribeiro (2011). SVR Controller for a Biped Robot with a Human-like Gait Subjected to External Sagittal Forces, Biped Robots, Prof. Armando Carlos Pina Filho (Ed.), ISBN: 978-953-307-216-6, InTech, Available from:

<http://www.intechopen.com/books/biped-robots/svr-controller-for-a-biped-robot-with-a-human-like-gait-subjected-to-external-sagittal-forces>

**INTECH**  
open science | open minds

#### **InTech Europe**

University Campus STeP Ri  
Slavka Krautzeka 83/A  
51000 Rijeka, Croatia  
Phone: +385 (51) 770 447  
Fax: +385 (51) 686 166  
[www.intechopen.com](http://www.intechopen.com)

#### **InTech China**

Unit 405, Office Block, Hotel Equatorial Shanghai  
No.65, Yan An Road (West), Shanghai, 200040, China  
中国上海市延安西路65号上海国际贵都大饭店办公楼405单元  
Phone: +86-21-62489820  
Fax: +86-21-62489821

© 2011 The Author(s). Licensee IntechOpen. This chapter is distributed under the terms of the [Creative Commons Attribution-NonCommercial-ShareAlike-3.0 License](#), which permits use, distribution and reproduction for non-commercial purposes, provided the original is properly cited and derivative works building on this content are distributed under the same license.

IntechOpen

IntechOpen